11th World Congress on Computational Mechanics (WCCM XI)
5th European Conference on Computational Mechanics (ECCM V)
6th European Conference on Computational Fluid Dynamics (ECFD VI)
E. Oñate, J. Oliver and A. Huerta (Eds)

NUMERICAL MODELING AND VALIDATION OF THE WIND FLOW OVER THE LAKE WANNSEE

Oliver Krüger[1*], Christina Schrödinger[1], Antonio Lengwinat[2], and Christian Oliver Paschereit[1]

[1] Chair of Fluid Dynamics – Hermann-Föttinger-Institut –, TU-Berlin, Müller-Breslau Str. 8, D-10623 Berlin, o.krueger@tu-berlin.de, www.fd.tu-berlin.de
[2] Fachgebiet Dynamik Maritimer Systeme, TU-Berlin, Salzufer 17-19, D-10587 Berlin, lengwinat@tu-berlin.de, www.dms.tu-berlin.de

Key words: Atmospheric Flows, Computational Fluid Dynamics (CFD), Tree Canopy, Complex Terrain.

Abstract. The present report focuses on the evaluation of wind flow over the lake *Wannsee* in Berlin, Germany. The goal was to validate the numerical models for flow over complex terrain for sailing applications. With this purpose simulations were conducted, and the large forests regions surrounding the lake were modeled with a displacement surface. In order to validate the simulations wind data was obtained on a sailing yacht. It is shown that the terrain has a significant influence on the flow field and even cape effects could be identified. It was found that simulations are in line with the measurements. Furthermore, the results show that the wind flow over complex terrain can be captured by using eddy viscosity based models.

1 Introduction

Predicting air flows over complex terrain is of high interest for a broad variety of applications. Determining the wind loads on wind turbines and the optimization of the deployment within a candidate wind farm location to maximize the power output are probably the most prominent applications in wind engineering. Other applications are the prediction of dispersion of pollutants or the evaluation of pedestrian level winds. Due to the fact that the atmospheric boundary layer (ABL) is the lowest part of the atmosphere, its flow pattern is mainly influenced by the ground topology.

There is extensive literature concerning computational fluid dynamics (CFD) simulations of wind flows over complex terrain. Comprehensive literature reviews may be found in Ref. [3, 8]. Most studies use a finite volume code based on solving the incompressible

*Address all correspondence to this author: *o.krueger@tu-berlin.de*

Reynolds averaged Navier-Stokes equations (RANS) together with a two-equation turbulence model (usually $k - \varepsilon$ [5, 12, 9]). RANS methods only provide information on the mean wind and turbulent kinetic energy level. However, they are favored due to their robustness and low computational costs. Nonetheless, *Large Eddy Simulations* (LES) are becoming more popular [23, 6].

Some comprehensive databases for model validation exist, such as the Askervein Hill project [21], the Kettles Hill project [18] or recently the Bolund Experiment [2]. However, most of these cases are without obstacles and focus on the flow over solid ground. Therefore, the present study is dedicated to the evaluation of the wind flow over the lake *Wannsee* in Berlin, Germany. The main goal is to validate the used models especially for the prediction of wind fields for sailing applications. Blocken [4] highlighted that a computational domain can usually be separated in three regions. The first two regions include, a down- and upstream region where obstacles are modeled implicitly in terms of surface roughness. In the third region the obstacles are modeled explicitly. Lake *Wannsee* is framed by deciduous forests and modeling every single tree is out of question. However, if individual roughness elements of a specific size are packed closely together, they act as a displacement surface. Taking this into account, the forest region was elevated by 80% of the average tree size ($\approx 14\,\mathrm{m}$) normal to the surface. The simulations were carried out with the free open source toolkit OpenFOAM (version 2.1.1) using the SST turbulence closure. In order to validate the simulations, measurements were conducted on a sailing yacht equipped with wind sensors (cup anemometer and wind vane) and a positioning system.

The paper is structured such that first, the investigated topography and the computational domain are presented. Second, the numerical models especially the boundary profiles and the displacement surface are explained in detail followed by the description of the measurement techniques. The results of the simulations are discussed and compared with the experimental data in section 6. Finally, the results are summarized and conclusions are drawn.

2 Terrain Representation

Wannsee is the name for a quarter and a lake southwest of Berlin, Germany (N52°25′ 39″ E13°10′ 23″). The quarter is surrounded by the river *Havel*, the lake *Großer Wannsee*, the lake *Kleiner Wannsee*, and some smaller lakes. Both lakes have a maximum depth of 9 m and are famous for bathing, water sports and sailing competitions. Figure 1 depicts a satellite image (right). As can be seen, the area consists of urban regions and large forests. The elevation of the topography is shown in the left image and was derived from a digital terrain model (DTM), which is computed from satellite data with a spatial resolution of 25 m. The water level was set to zero and the highest elevation is approximately 80 m above the water. The deciduous forests consists mainly of oaks and pines and are marked in orange in the center image of Fig. 1.

For the simulations the map was divided in three layers, a water layer, a forest layer and

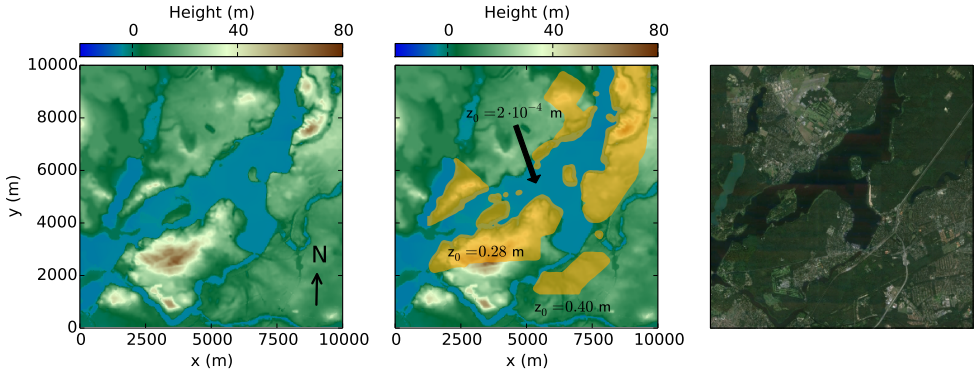

Figure 1: Overview of the computational domain showing the discretized topography (left), the displaced forest-layer (middle), and a satellite image (right) taken from Google Maps (accessed May 2013).

an urban layer which contains the remaining areas. For each layer a different aerodynamic roughness lengths was used. The roughness parameters are further explained later on. The simulations were conducted on a rectangular domain with a quadratic base area of 10 x 10 km and a height of 500 m above the water level.

3 Numerical Modeling

The motion of an isothermal and incompressible fluid can be described by the conservation of mass and momentum. The incompressible *Reynolds averaged Navier-Stokes* equations are used to simulate the turbulent flow field:

Continuity ($i = 1, 2, 3$):

$$\frac{\partial \left(u_i\right)}{\partial x_i} = 0\,. \tag{1}$$

Reynolds averaged Navier-Stokes ($i = 1, 2, 3$):

$$\varrho \left(\frac{\partial \overline{u_i}}{\partial t} + \overline{u_j} \frac{\partial \overline{u_i}}{\partial x_j} \right) = -\frac{\partial \overline{p}}{\partial x_i} + \frac{\partial}{\partial x_j} \mu \left(\frac{\partial \overline{u_i}}{\partial x_j} + \frac{\partial \overline{u_j}}{\partial x_i} \right) - \frac{\partial \varrho \overline{u_i' u_j'}}{\partial x_j}, \tag{2}$$

where u_i represents the velocity component, ϱ the density, p the pressure, μ the dynamic viscosity, and t the time. In the present study the *Shear Stress Transport* (SST) model by Menter [13] was employed, because it is a good compromise of accuracy, robustness and computational costs.

The simulations were conducted using the open-source framework OpenFOAM 2.1.1. As a solver *simpleFoam* was used. It is a steady-state, incompressible, isothermal solver for turbulent flows. The pressure-velocity coupling is performed applying the SIMPLE algorithm as described by Patankar [16], ensuring that continuity is satisfied. The balance equations were solved using a second-order implicit scheme. Dirichlet boundary conditions

are enforced at the inlet for all variables except for the pressure, which uses a zero-gradient condition (Neumann). Similarly, the outflow is treated using zero-gradient for all variables. To account for surface roughness of the terrain, rough-wall functions were applied. The computational grid used in the present study, consists of unstructured tetrahedral cells with a boundary layer refinement. A core area of 5x5 km was refined to feature cell edge length of $\approx 20\,\mathrm{m}$. The boundary layer refinement resulted in 10 prism layers and a distance from the wall-adjacent cell center to the bottom of the domain of 50 cm. The grid insensitivity was tested beforehand and the final grid consist of 3.2 million cells.

4 Boundary Conditions

4.1 Atmospheric Boundary Layer Profile

The inlet boundary profile was modeled by a rough surface approach, based on a log-law tangential velocity u:

$$u(z) = \frac{u^*}{\kappa} \cdot \ln\left(\frac{z}{z_0}\right), \tag{3}$$

where $\kappa = 0.4$ is the Kármán constant, u^* is the friction velocity, z the distance above the ground and z_0 a characteristic atmospheric roughness length. According to Panofsky and Dutton [15] the formulation represents wind profiles up to 150 m for homogeneous terrain appropriately. For a preliminary study Askervein Hill [21] was investigated, for which a large body of literature exists. It was found that the wind profile resulting from Eq. 3 is in good agreement up to a height of 400 m. Therefore we assume that the profile is suitable to represent flow conditions in the present study. An additional set of inlet conditions was applied as suggested by Blocken [4]:

$$k = \frac{u^{*2}}{\sqrt{C_\mu}} \tag{4}$$

$$\varepsilon = \frac{u^{*3}}{\kappa \cdot (z + z_0)} \tag{5}$$

$$\omega = \frac{u^*}{\kappa\sqrt{C_\mu(z + z_0)}}. \tag{6}$$

Here, k is the turbulent kinetic energy, ε the eddy dissipation, ω the specific dissipation, and $C_\mu = 0.09$ a model constant. This set of inlet profiles fulfills the conditions of Richards and Hoxey [17, 14] for a self-sustaining ABL.

4.2 Wall Functions

For modeling rough walls a wall function (*nutkRoughWallFunction*) is applied to compute the wall shear stress:

$$\frac{u_p}{u^*} = \frac{1}{\kappa} \ln\left(\frac{E z_p}{C_s k_s}\right), \tag{7}$$

where $E \approx 9.793$ is the wall constant, $C_s = 0.327$ a roughness constant, z_p the distance to the cell center of the first wall adjacent cell, and u_p the velocity in the cell center. The friction velocity u^* is computed from the turbulent kinetic energy:

$$u^* = C_\mu^{0.25} \cdot k^{0.5}. \tag{8}$$

The roughness length k_s was modeled according to Blocken [4]:

$$k_s = 30 \cdot z_0. \tag{9}$$

4.3 Displacement Surface

The computational domain was derived from satellite data, which does not comprise obstacles such as trees and buildings. As can be seen in the satellite picture in Fig. 1 (right) the lake Wannsee is surrounded by deciduous forests. The presence of packed groups of trees can affect the wind flow in a region to an extent that they act as a single obstacle. Figure 2 illustrates the flow over forest canopy. Compared to the undisturbed surface flow (red curve), the thick canopy layer acts as a rough surface at a position where half of the tangential momentum diminishes. Thus, a displacement distance d and a reduced surface roughness z_0 may be attributed to this surface.

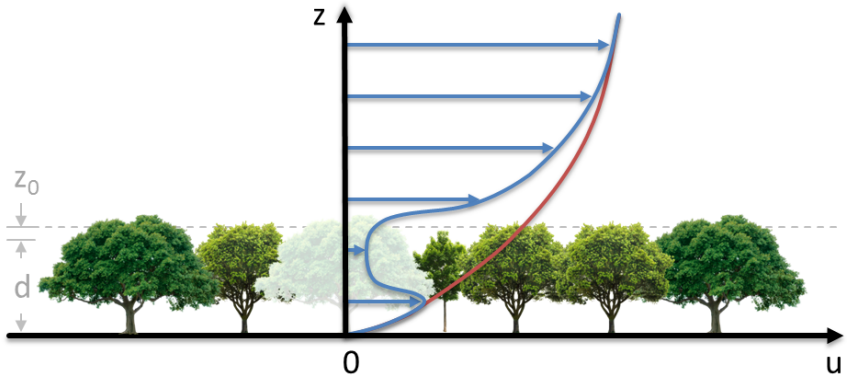

Figure 2: Flow over forest canopy showing the wind profile (blue curve) as a function of the height z. Compared to an undisturbed surface flow (red curve), the thick canopy layer acts as surface with a displacement distance d and a reduced surface roughness z_0. Schematic according to Ref. [20].

In order to evaluate the zero plane displacement distance d and the roughness length z_0, the determination of the eddy-correlation of the Reynolds stresses can be iteratively solved [10]. However, a more convenient method of deriving d and z_0 is by introducing the replacement height d to the neutral wind profile in Eq. 3:

$$u = \frac{u^*}{\kappa} \ln\left(\frac{(z-d)}{z_0}\right). \tag{10}$$

Although this formulation may match observed wind profiles close to a layer of vegetation, it must be considered as an empirical model and does not necessarily yield the correct value of the vertical drag force [19]. Nevertheless, Baldocchi and Meyers [1] reported a good agreement of Eq. 10 for the flow over a deciduous forest. To determine the replacement height d, Hicks and coworkers [10] measured the flow over a plantation of *Pinus radiata* with an average height of $12.4 \pm 1.2\,\mathrm{m}$ and derived from the Reynolds stresses and the wind speed gradients that the location of the zero plane for momentum is located at 80% of the average tree height. Dolman [7] reported it is about 75% of the average tree height (9.6 m) for a European oak forest. On the other hand, Baldocchi and Meyers [1] concluded for a flow over an uneven aged forest of mainly oak and hickory trees with an average height of about 23 m a factor of 90%. The deciduous forest surrounding lake Wannsee consists mainly of pines (56%) and oaks (26%) with some occasional birches and beeches. From observations, an average tree height of $h = 14\,\mathrm{m}$ was estimated. A factor of 80% of the average tree size for the replacement height was assumed, due to the fact that the tree height of Hicks' findings [10] is comparable to our conditions. From this, the replacement height d is:

$$d = 0.8 \cdot h = 11.2\,\mathrm{m}. \tag{11}$$

The reduced roughness length z_0 can be determined by a correlation of Kondo and Yamazawa [11], which relates the total area S covered by the trees with the sum of the roughness elements' heights h_i and the area of the obstacles s_i:

$$z_0 = \frac{1}{4S} \sum h_i s_i. \tag{12}$$

For simplicity, it is assumed that the trees are evenly distributed. This would lead to a remaining tree height of $(h-d)$. Taking now into account that the trees are probably not overall evenly distributed and that the estimated tree height neglected some smaller trees, a corrected remaining tree height of $1/2(h-d)$ is assumed. Assuming that all trees have the same width and that the treetops cover 80% of the total area leads to a simplified expression:

$$z_0 = \frac{1}{4S} \sum h_i s_i \approx \frac{1}{4} \cdot \frac{1}{2} (h-d) \cdot \frac{4}{5} = 0.28\,\mathrm{m}. \tag{13}$$

With the evaluation of the displacement height d and the according atmospheric roughness length z_0 the forest areas were elevated by 80% of the average tree size ($\approx 14\,\mathrm{m}$) normal to the surface, as shown in orange in the right image in Fig. 1. The transition between the elevated and the non-forest areas was modeled linearly. The atmospheric roughness lengths for the complete domain are summarized in Tab. 1. The roughness for the urban region and water was taken from Ref. [22].

Table 1: Settings of the roughness length and replacement height for the computational domain.

Region	Atmospheric roughness length z_0 (m)	Replacement height d (m)
Urban	0.4	0
Forest	0.28	11.2
Water	$2 \cdot 10^{-4}$	0

5 Experimental Setup

The measurements were conducted on a *8m One Design* sailing yacht, as depicted in Fig. 3(a). The yacht was equipped with wind measuring devices in the scope of a lecture at the Chair of Fluid Dynamics, TU Berlin. The combination of a GPS device and the measurement of the apparent wind allows for the determination of the true wind at the mast top during a measuring run for every position. The measuring device mounted at the mast top consists of a cup anemometer, a GPS device, a NMEA interface, and a data logger as shown in Fig. 3(b). In order to ensure reasonable measurements, the anemometer was calibrated in a laminar wind tunnel.

Each wind field assessment over complex terrain should be based on a comprehensive wind analysis, in order to select the most relevant wind field situation. More than 33 measuring runs were conducted and two runs were selected based on the most dominant wind direction. The predominant wind direction during the measurements was between west and southwest ($225° - 270°$). Unfortunately, the quarter is well known for its high wind gusts. Two measuring runs were chosen. The first case was conducted on the 4^{th} of June 2010 and the dominant wind direction was 270°. In the following, the case is denoted as "040610". The second case features a dominant wind direction of 245° and was conducted on the 11^{th} of June 2010. Hence, the case is denoted as "110610".

Figure 4 illustrates the sailing paths for both measurement runs. Both measurements started at the marina at the lake *Großer Wannsee* into the river *Havel*. The short run (case "040610") took about 28 min and the other run took about 157 min. Both runs were affected by transient wind conditions (e.g., wind gusts, wind shifts) and other water vehicles (e.g., ferries, wind surfers, sailing yachts). For both cases, the wind direction and velocity, and position were recorded as a function of time with a sampling rate of 1 Hz. The data was processed and all turns were omitted to prevent errors induced by

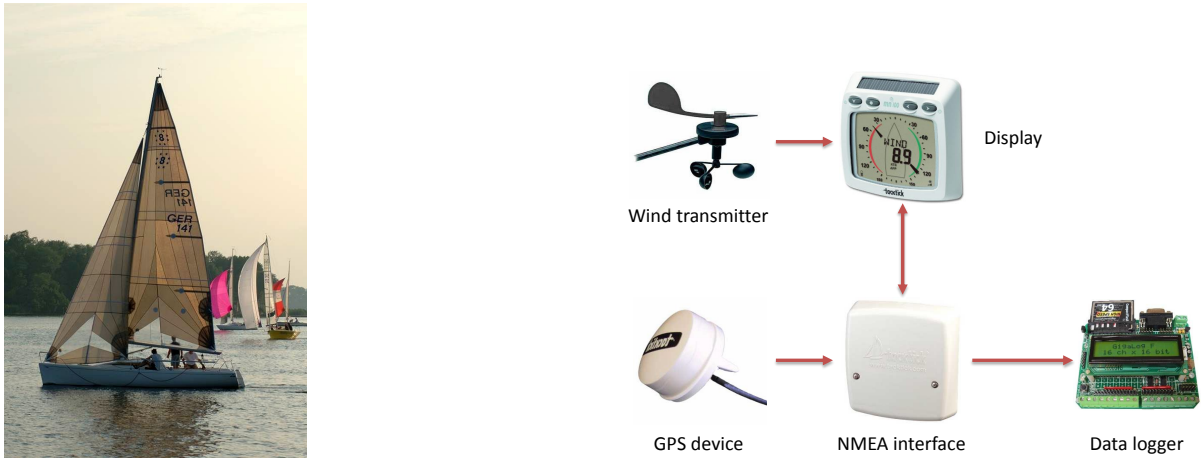

(a) Sailing yacht. (b) Measuring equipment.

Figure 3: The figure depicts the sailing yacht for the wind measurements (left) and the mast top mounted measuring devices (right).

the sudden tumbling movement of the mast.

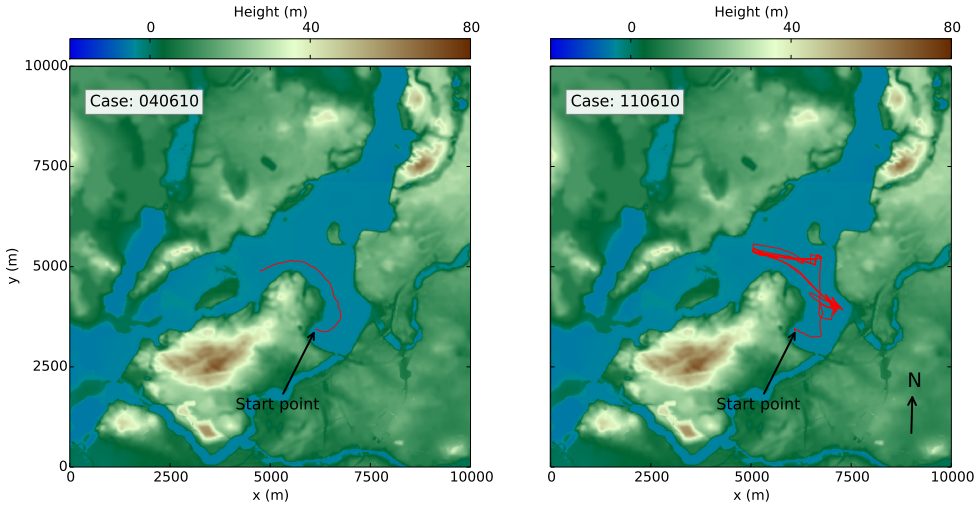

Figure 4: Tracks of the measuring runs for both cases.

The average wind conditions for both runs are listed in Tab. 2, and stem from a weather station at lake Wannsee operated by the *Freie Universität Berlin*.

6 Results and Discussion

The input parameters for both simulations were set according to the wind conditions and the aforementioned inlet profiles. As convergence criterion a maximum residual for all balances was set to 10^{-4} resulting in less than 4000 iterations. Neither convergence

Table 2: Wind conditions for both cases from the weather station at the Wannsee

	Case 040610	Case 110610
Mean velocity ($^{m}/_{s}$)	3	6
Max. wind gusts ($^{m}/_{s}$)	5	11
Wind direction (°)	270	245

problems nor periodic fluctuations of the residua, indicating large scale vortices, were observed. Figure 5 depicts the computed distribution of the velocity magnitude for both

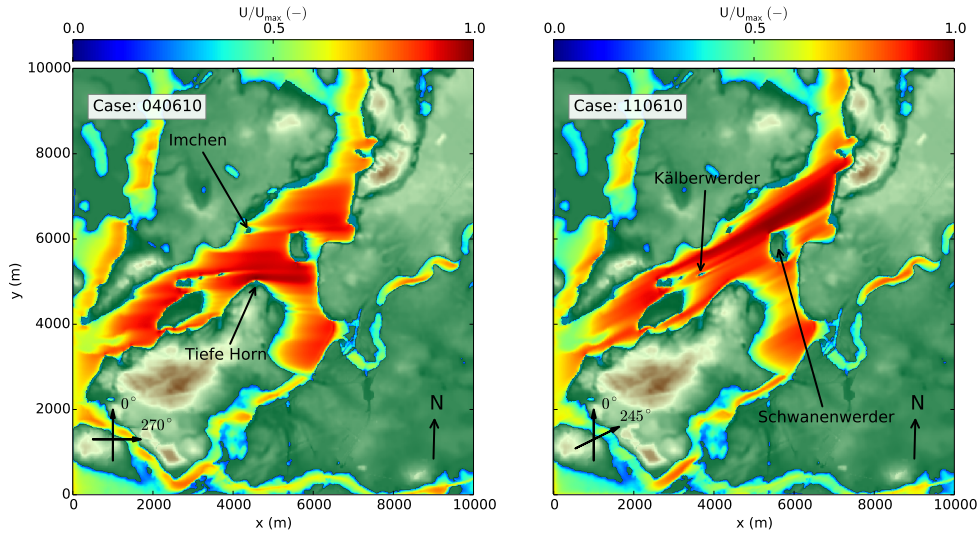

Figure 5: Computed velocity magnitude distribution for both cases 10 m above the water surface. The colormap for the terrain is identical to the other plots and may be found in Fig. 4.

cases in a plane 10 m above the water level. For both cases a speed-up over the water layer is observed, which stems from the small roughness value. The accelerated flow causes wakes with low velocities and high gradients when passing islands (e.g., *Imchen*, *Schwanenwerder*, *Kälberwerder*). Moreover, a strong impact of the terrain is observed on the flow, resulting in bands of quasi constant velocities. In the case of west wind (270°), a bending of the flow downstream of cape *Tiefe Horn* is detected. This cape effect is caused by a lower pressure region at the lee side of the cape causing a curvature of the streamlines towards the cape. For the other case ("110610"), the same effect can be observed at the cape of the peninsula *Schwanenwerder*. The cape effect at southwest wind is well known and can be beneficial when attending a sailing regatta. A comparison of the measured and simulated data is given in Fig. 6. There, the normalized measured velocity is plotted as a function of time corresponding to locations on the lake. In order to draw a comparison the computed normalized velocity extracted from a plane 10 m above the

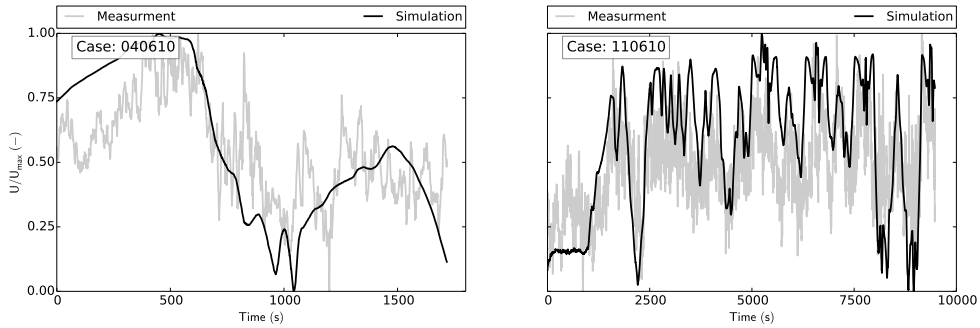

Figure 6: Velocity profile as a function of the sailing time. A distinct time corresponds to a distinct position on the sailing course.

water is superimposed on the experimental data. The velocities were normalized with the maximum velocity to account for slightly different wind conditions. For both cases a high fluctuation of the measured velocity can be observed, which is directly related to the high wind gusts registered by the weather station (see Tbl. 2) and the movement of the mast. In the case "040610" (Fig. 6 left), a smooth trend of the velocity is predicted, which is due to the fact that the simulation did not take wind gusts into account. Compared to the measurement the computed velocity field reflects the overall trend and is beside the high gusts well in line with the measurements. For the other case "110610" (Fig. 6 right), a similar outcome is observed. Again, the simulation is not capable of predicting the high wind gusts. For some positions (e.g., 2000 s-4800 s) the minima are overestimated and it seems that there is an overall offset. However, the maxima are well predicted. This deviation cannot be fully explained here, because different reasons are possible. Due to the fact that an average wind direction and magnitude were used as input parameters, wind shifts cannot be regarded, which are likely at a windy day. However, the simulation is able to predict the overall trends.

7 Conclusion

In this study a wind flow over the complex terrain of lake *Wannsee* in Berlin, Germany was evaluated. The goal was to validate computational models especially for the prediction of wind fields for sailing applications. Due to the fact that the lake is framed by deciduous forests and closely packed obstacles act as a displacement surface, the forest regions were elevated by 80% of the average tree height. The simulations were carried out with a SST turbulence closure. In order to validate the simulations, measurements were conducted on a sailing yacht equipped with wind sensors and a positioning system.

It was found that in contrast to preliminary studies, the forests have a significant impact on the flow field. Wakes with high gradients were observed downstream of islands and even cape effects were identified. Compared to the measurements it was revealed that the computations are not capable of predicting wind gusts, but are able to represent the overall trends of the wind field and also captures the extrema of the wind profiles.

Moreover, it can be stated that it is possible to reproduce the trends of a wind flow over complex terrain with steady-state simulations, even though wind gusts and shifts are neglected.

REFERENCES

[1] Dennis D. Baldocchi and Tilden P. Meyers. Turbulence Structure in Deciduous Forest. *Boundary-Layer Meteorology*, 43:345–364, 1988.

[2] J. Berg, J. Mann, A. Bechmann, M. S. Courtney, and H. E. Jø rgensen. The Bolund Experiment, Part I: Flow Over a Steep, Three-Dimensional Hill. *Boundary-Layer Meteorology*, 141(2):219–243, July 2011.

[3] G. T. Bitsuamlak, Ted Stathopoulos, and C. Bédard. Numerical Evaluation of Wind Flow over Complex Terrain: Review. *Journal of Aerospace Engineering*, 17(4):135–145, October 2004.

[4] B. Blocken, T. Stathopoulos, and J. Carmeliet. CFD simulation of the atmospheric boundary layer: wall function problems. *Atmospheric Environment*, 41(2):238–252, January 2007.

[5] F. A. Castro, J. M. L. M. Palma, and A. Silva Lopes. Simulation of the Askervein Flow. Part 1: Reynolds Averaged Navier Stokes Equations (k-epsilon Turbulence Model). *Boundary-Layer Meteorology*, (1996):501–530, 2003.

[6] F. A. Castro, J. M. L. M. Palma, and A. Silva Lopes. Simulation of the Askervein flow. Part 2: Large-eddy simulations. *Boundary-Layer Meteorology*, 125(1):85–108, July 2007.

[7] A. J. Dolman. Estimates of roughness length and zero plane displacement for a foliated and non-foliated oak canopy. *Agricultural and Forest Meteorology*, 36(3):241–248, February 1986.

[8] Kemal Hanjalić and Saša Kenjereš. Some developments in turbulence modeling for wind and environmental engineering. *Journal of Wind Engineering and Industrial Aerodynamics*, 96(10-11):1537–1570, October 2008.

[9] D. M. Hargreaves and N. G. Wright. On the use of the k-epsilon model in commercial CFD software to model the neutral atmospheric boundary layer. *Journal of Wind Engineering and Industrial Aerodynamics*, 95(5):355–369, May 2007.

[10] B. B. Hicks, P. Hyson, and C. J. Moore. A Study of Eddy Fluxes Over a Forest. *Journal of Applied Meteorology*, 14:58–66, 1974.

[11] Junsei Kondo and Hiromi Yamazawa. Aerodynamic Roughness over an Inhomogeneous Ground Surface. *Boundary-Layer Meteorology*, 35(1983):331–348, 1986.

[12] N. Mandas, F. Cambuli, G. Crasto, and G. Cau. Numerical simulation of the Atmospheric Boundary Layer (ABL) over complex terrains. *European Wind Energy Conference & Exhibition 2004*, pages 1–11, 2004.

[13] Florian R. Menter. Two-equation eddy-viscosity turbulence models for engineering applications. *AIAA journal*, 32(8):1598–1605, 1994.

[14] S. E. Norris and P. J. Richards. Appropriate boundary conditions for computational wind engineering models revisited. *Journal of Wind Engineering and Industrial Aerodynamics*, 99(4):257–266, April 2011.

[15] H. A. Panofsky and J. A. Dutton. *Atmospheric turbulence: models and methods for engineering applications*. A Wiley interscience publication. John Wiley & Sons, Somerset, NJ, 1984.

[16] S. V. Patankar and D. B. Spalding. A calculation procedure for heat, mass and momentum transfer in three-dimensional parabolic flows. *International Journal of Heat and Mass Transfer*, 15(10):1787–1806, October 1972.

[17] P. J. Richards and R. P. Hoxey. Appropriate boundary conditions for computational wind engineering models using the k- turbulence model. *Journal of Wind Engineering and Industrial Aerodynamics*, 46-47:145–153, August 1993.

[18] J. R. Salmon, H. W. Teunissen, R. E. Mickle, and P. A. Taylor. The Kettles Hill Project: Field observations, wind-tunnel simulations and numerical model predictions for flow over a low hill. *Boundary-Layer Meteorology*, 43(4):309–343, June 1988.

[19] Roger H. Shaw and A.R. Pereira. A numerical experiment on the mean wind structure inside canopies of vegetation. *Agricultural Meteorology*, 22(3-4):303–318, December 1980.

[20] Roland B. Stull. *An Introduction to Boundary Layer Meteorology*. Springer Netherlands, Dordrecht, 1988.

[21] P. A. Taylor and H. W. Teunissen. Askervein '82: Report on the September / October 1982 Experiment to Study Boundary Layer Flow over Askervein, South Uist. Technical report, Atmospheric Environment Service, Ontario, 1982.

[22] I. Troen and E. L. Petersen. *European Wind Atlas*. RisøNational Laboratory, Roskilde, 1989.

[23] N. Wood. Wind flow over complex terrain: a historical perspective and the prospect for large-eddy modelling. *Boundary-Layer Meteorology*, 96:11–32, 2000.